Multigroup Neutral Particle Transport Theory Revisited: The Development of an Analytical Benchmark

B. D. Ganapol[†]
Department of Aerospace and Mechanical Engineering
University of Arizona
Ganapol@cowboy.ame.arizona.edu

Abstract

The multigroup equation of neutron transport theory is solved in an infinite medium setting to obtain the partial Green's function. The solution is found via a Fourier transform approach from which the singular eigenfunction expansion emerges. The solution features full anistropic scattering and a full group-to-group scattering matrix. As a demonstration, the scalar flux for several scenarios is obtained both in plane and spherical geometries. The application of the Wynn-epsilon acceleration algorithm is shown to provide remarkable improvement for highly forward-peaked scattering.

1. Introduction

In the past, considerable attention was given to demonstrating that a theory of singular eigenfunctions existed for the solution to the multigroup transport equation[1-6]. This activity was a natural outgrowth of the many investigations concerning the one-group case that had been so elegantly treated by Case and Zweifel[7]. Some of the earliest considerations relied on knowledge of the solution form before attempting a theory. In other words, the form of the singular eigenfunction solution had to be guessed. In reviewing early attempts to develop a full-range multigroup singular eigenfunction expansion for general anisotropic scattering, the achievements, at best, were rather disappointing. No explicit theory had been put forth until 1976 when, in a seminal work, the Larsen-Habetler technique was applied to the multigroup case with isotropic scattering[8,9]. Anisotropic scattering was not treated however. The primary motivation for this presentation is to show that a multigroup full-range expansion can indeed be obtained for the partial Green's function in plane geometry from the Fourier transform approach. The curiosity here is that the solution can be found without resorting to the relatively obscure mathematics associated with singular eigenfunctions and resolvant operators. In addition, the Fourier transform approach yields a convenient expression of the solution suitable for numerical evaluation in a variety of geometrical settings as will be demonstrated.

A firmly established Fourier transform theory, paralleling that of the one-group case, will be presented for an isotropically emitting source in the multigroup plane geometry approximation. Then by using the resulting image function in a numerical Fourier transform inversion, analytical benchmark quality scalar fluxes will be obtained in both plane and spherical geometries.

In one-group transport theory, it is well known that the solution to the transport equation in an infinite medium obtained via singular eigenfunctions and from Fourier transforms

[†] Work performed under a DoE NEER grant

are identical for isotropic scattering. When higher order scattering is considered, the correspondence was not at all apparent until recently [10,12]. In reference 10, it was shown that the Fourier transform image function leads to the singular eigenfunction solution when analytically continued into the complex plane even for general anisotropic scattering. It is the intent of this presentation to apply similar reasoning to the multigroup case (limited to isotropic source emission) in order to extend the fundamental theoretical development of linear transport theory and partially "close the loop". In the process, as in reference 10, an image function appropriate for numerical inversion is obtained allowing for an accurate numerical evaluation of the partial Green's function in plane and associated geometries.

2. Fourier Transform Solution

We begin with the following special form of the multigroup transport equation for the partial Green's function in an infinite medium (isotropic source emission):

$$\left[\mu \underline{I}\frac{\partial}{\partial x}+\underline{\Sigma}\right]\vec{\Psi}(x,\mu)=\frac{1}{2}\sum_{l=0}^{L}P_l(\mu)\underline{C}_l\vec{\Psi}_l(x)+\frac{1}{2}\delta(x)\vec{q} \qquad (1a)$$

for G groups. The Legendre moment vectors are defined as

$$\vec{\Psi}_l(x)\equiv\int_{-1}^{1}d\mu P_l(\mu)\vec{\Psi}(x,\mu), \qquad (1b)$$

and the boundary condition is

$$\lim_{|x|\to\infty}\vec{\Psi}(x,\mu)<\infty\ . \qquad (1c)$$

The group-to-group transfer matrix is $\underline{C}_l$ and the source vector $\vec{q}$ can include sources in all G groups

$$\vec{q}\equiv[q_1,q_2,...,q_G]^T\ .$$

An underbar, i.e., $\underline{M}$, indicates a matrix quantity. $\vec{\Psi}(x,\mu)$ is the G-component angular flux vector; and for theoretical convenience, the G-group parameters have been normalized such that the original total cross section of group g (s_g) is expressed as

$$\sigma_g\equiv s_g/s_{min}\geq 1$$
$$s_{min}\equiv \min_{1\leq g\leq G}\left(s_g\right)$$

with the total cross section matrix represented by

$$\underline{\Sigma}\equiv diag\left[\sigma_g\right].$$

The Legendre scattering coefficients have also been appropriately modified. Also, the spatial coordinate has been changed to the dimensionless coordinate

$$x \to x\, s_{min} \ .$$

Eq(1a) can be recast into the fundamental matrix form

$$\left[\mu \underline{I} \frac{\partial}{\partial x} + \underline{\Sigma}\right] \underline{\Psi}(x,\mu) = \frac{1}{2} \sum_{l=0}^{L} P_l(\mu) \underline{C}_l \underline{\Psi}_l(x) + \frac{1}{2} \delta(x) \underline{I} \quad (2a)$$

where

$$\vec{\Psi}(x,\mu) = \underline{\Psi}(x,\mu)\, \vec{q} \quad (2b)$$

and now $\underline{\Psi}(x,\mu)$ is the solution matrix. With the application of the Fourier transform,

$$\underline{\Psi}(k,\mu) \equiv \int_{-\infty}^{\infty} dx\, e^{ikx}\, \underline{\Psi}(x,\mu) \ , \quad (3)$$

eq(2a) can be algebraically solved to give

$$\underline{\Psi}(k,\mu) = \frac{1}{2}\left[\underline{\Sigma} - ik\mu \underline{I}\right]^{-1} \sum_{l=0}^{L} P_l(\mu) \underline{C}_l \underline{\Psi}_l(k) + \frac{1}{2}\left[\underline{\Sigma} - ik\mu \underline{I}\right]^{-1} . \quad (4)$$

In the following, a function of *k* or *z* will denote a Fourier transform.

The representation of the transformed angular flux given by eq (4) is central to the analysis to follow. It will subsequently be shown that the Fourier transform inversion

$$\underline{\Psi}(x,\mu) \equiv \frac{1}{2\pi} \int_{-\infty}^{\infty} dk\, e^{-ikx}\, \underline{\Psi}(k,\mu) \ , \quad (5)$$

leads to the singular eigenfunction expansion. The approach taken is to specify the moments $\underline{\Psi}_l$ used to reconstruct $\underline{\Psi}$ from its Legendre polynomial expansion.

In the usual way, projection over Legendre polynomials on the interval [-1,1] gives a set of moment equations

$$\underline{\Psi}_j(k) = z \sum_{l=0}^{L} \underline{V}_{jl}(z\underline{\Sigma}) \underline{C}_l \underline{\Psi}_l(k) + z\ \underline{V}_{j0}(z\underline{\Sigma}) \quad (6a)$$

where

$$\underline{V}_{jl}(z\underline{\Sigma}) = \underline{V}_{lj}(z\underline{\Sigma}) \equiv \frac{1}{2} \int_{-1}^{1} d\mu P_j(\mu) P_l(\mu) \underline{D}(z,\mu) \quad (6b)$$

with

$$\underline{D}(z,\mu) \equiv [z\underline{\Sigma} - \mu \underline{I}]^{-1} \ .$$

Also, the new independent variable z has been defined as

$$z \equiv 1/ik$$

giving the true functional relation of the solution to eq(6a) as

$$\underline{\Psi}_l(k) \equiv \underline{\Psi}_l(z) \ .$$

Note that the (diagonal) matrix Legendre function of the second kind is defined by

$$\begin{aligned} \underline{Q}_l(z\underline{\Sigma}) &\equiv \underline{V}_{0l}(z\underline{\Sigma}) = diag\left[Q_l(z\sigma_1),...,Q_l(z\sigma_G)\right] \\ &= diag\left[\frac{1}{2}\int_{-1}^{1} d\mu \frac{P_l(\mu)}{z\sigma_g - \mu}\right]. \end{aligned} \tag{7}$$

The matrix inversion of eq(6a), in essence, provides the desired moment transforms; but essential features of the solution are masked in so doing. For this reason, only the specific case, $j = 0$ is considered

$$\underline{\Psi}_0(z) = z \sum_{l=0}^{L} \underline{Q}_l(z\underline{\Sigma}) \underline{C}_l \underline{\Psi}_l(z) + z\underline{Q}_0(z\underline{\Sigma}) \tag{8}$$

which is to be supplemented by moment equations. The last equation can be written more concisely as

$$\sum_{l=0}^{L} \left[\delta_{l,0}\underline{I} - z\underline{Q}_l(z\underline{\Sigma})\underline{C}_l\right]\underline{\Psi}_l(z) = z\,\underline{Q}_0(z\underline{\Sigma}) \ . \tag{9}$$

A second set of moment equations is obtained by projection of eq(2a) over

$$[z\underline{\Sigma} - \mu \underline{I}]P_j(\mu)$$

on the interval [-1,1]. In the usual way, from the well known recurrence relation for Legendre polynomials

$$(2l+1)\mu P_l(\mu) = (l+1)P_{l+1}(\mu) + lP_{l-1}(\mu), \tag{10}$$

a recurrence relation for the moments results for $0 \le l \le L$

$$-z\underline{h}_l\underline{\Psi}_l(z)+(l+1)\underline{\Psi}_{l+1}(z)+l\underline{\Psi}_{l-1}(z)=-(2l+1)z\delta_{l,0} \qquad (11a)$$

where

$$\underline{h}_l \equiv (2l+1)\underline{\Sigma}-\underline{C}_l \ . \qquad (11b)$$

The general, solution to this recurrence relation can be formulated as

$$\underline{\Psi}_l(z)=\underline{G}_l(z)\underline{\Psi}_0(z)-\underline{\rho}_l(z) \qquad (12)$$

where the matrix G-and ρ- polynomials satisfying

$$\begin{gathered}-z\underline{h}_l\underline{G}_l(z)+(l+1)\underline{G}_{l+1}(z)+l\underline{G}_{l-1}(z)=0 \\ \underline{G}_0(z)\equiv\underline{I}\end{gathered} \qquad (13a)$$

$$\begin{gathered}-z\underline{h}_l\underline{\rho}_l(z)+(l+1)\underline{\rho}_{l+1}(z)+l\underline{\rho}_{l-1}(z)=z\delta_{l0}\underline{I} \\ \underline{\rho}_0(z)\equiv\underline{0}\end{gathered} \qquad (13b)$$

have been introduced. It should be noted that an entirely parallel procedure to the one-group case is being followed here. $\underline{\Psi}_0(z)$ is obtained by substitution of the moment representation of eq(12) into eq(9) to give

$$\underline{\Psi}_0(z)=\underline{\Lambda}_L^{-1}(z)\underline{\hat{g}}_L(z) \qquad (14a)$$

or more explicitly

$$\begin{aligned}\underline{\Psi}_0(z)=\left[\underline{Q}_L(z\underline{\Sigma})\,\underline{G}_{L+1}(z)-\underline{Q}_{L+1}(z\underline{\Sigma})\,\underline{G}_L(z)\right]^{-1}\bullet \\ \bullet\left[\underline{Q}_L(z\underline{\Sigma})\underline{\rho}_{L+1}(z)-\underline{Q}_{L+1}(z\underline{\Sigma})\underline{\rho}_L(z)\right].\end{aligned} \qquad (14b)$$

To obtain eq(14b), the recurrence relation for $\underline{G}$ and $\underline{\rho}$ were used to condense the resulting expressions to those shown. Eq(14b) will serve as the kernel from which all numerical results will come.

3. Singular Eigenfunction Solution

We now consider the homogeneous form of eq(2a)

$$\left[\mu\underline{I}\frac{\partial}{\partial x}+\underline{\Sigma}\right]\underline{\Phi}(x,\mu)=\frac{1}{2}\sum_{l=0}^{L}P_l(\mu)\underline{C}_l\underline{\Phi}_l(x) \ . \qquad (15)$$

After a Fourier transform, eq(15) becomes

$$\left[\underline{\Sigma} - ik\mu\underline{I}\right]\underline{\Phi}(z,\mu) = \frac{1}{2}\sum_{l=0}^{L} P_l(\mu)\underline{C}_l\underline{\Phi}_l(z) \qquad (16)$$

and upon projection over Legendre polynomials, we find

$$-z\underline{h}_l\underline{\Phi}_l(z) + (l+1)\underline{\Phi}_{l+1}(z) + l\underline{\Phi}_{l-1}(z) = \underline{0} \ . \qquad (17)$$

Since we began with a homogeneous equation, the normalization

$$\underline{\Phi}_l(z) \equiv \underline{I}$$

can be defined in which case it is clear that

$$\underline{\Phi}_l(z) = \underline{G}_l(z) \ . \qquad (18)$$

It is now convenient to construct the Legendre polynomial representation of $\underline{\Phi}(z,\mu)$ as

$$\underline{\Phi}(z,\mu) = \sum_{l=0}^{\infty}\left(\frac{2l+1}{2}\right)\underline{G}_l(z)P_l(\mu) \ . \qquad (19)$$

When eq(19) is introduced into the Legendre polynomial representation of $\underline{\Psi}(z,\mu)$

$$\underline{\Psi}(z,\mu) = \sum_{l=0}^{\infty}\left(\frac{2l+1}{2}\right)\underline{\Psi}_l(z)P_l(\mu) \ , \qquad (20)$$

there results

$$\underline{\Psi}(z,\mu) = \underline{\Phi}(z,\mu)\underline{\Psi}_0(z) - \underline{R}(z,\mu) \qquad (21a)$$

where

$$\underline{R}(z,\mu) \equiv \sum_{l=0}^{\infty}\left(\frac{2l+1}{2}\right)\underline{\rho}_l(z)P_l(\mu) \ . \qquad (21b)$$

It should be emphasized that both $\underline{\Phi}(z,\mu)$ and $\underline{R}(z,\mu)$ are distributions when z is taken on the real line.

An alternative form for $\underline{\Phi}(z,\mu)$ can be obtained from the solution of eq(16), which takes some special care. In particular, the solution can be written as

$$\underline{\Phi}(z,\mu)=\frac{z}{2}[z\underline{\Sigma}-\mu\underline{I}]^{-1}\sum_{l=0}^{L}P_l(\mu)\underline{C}_l\underline{\Phi}_l(z)+\underline{\delta}(z,\mu)\underline{\Lambda}_L(z) \qquad (22a)$$

where

$$\underline{\delta}(z,\mu)\equiv\sum_{l=0}^{\infty}\left(\frac{2l+1}{2}\right)\underline{P}_l(z\underline{\Sigma})\underline{P}_l(\mu\underline{I}) \qquad (22b)$$

with

$$\underline{P}_l(z\underline{D})\equiv diag\left[P_l(zd_1),...,P_l(zd_G)\right] \qquad (22c)$$

for the diagonal matrix $\underline{D}$. In addition, $\underline{P}_l(z\underline{\Sigma})$ satisfies the recurrence

$$(2l+1)z\underline{\Sigma}\underline{P}_l(z\underline{\Sigma})=(l+1)\underline{P}_{l+1}(z\underline{\Sigma})+l\underline{P}_{l-1}(z\underline{\Sigma}), \qquad (23)$$

and the normalization of $\underline{\Phi}(z,\mu)$ to 1 has been used. Note that the second term of the solution comes from the condition

$$[z\underline{\Sigma}-\mu\underline{I}]\delta(z,\mu)=0$$

and that on the real line ($-\infty<\nu<\infty$))

$$\underline{\delta}(\nu,\mu)=diag[\delta(\sigma_1\nu-\mu),\delta(\sigma_2\nu-\mu),...\delta(\sigma_G\nu-\mu)] .$$

We are now in position to specify the Fourier inversion of eq(21a) noting that $\underline{\Phi}(z,\mu)$ is analytic [see eq(19)] and $\underline{\Psi}_0(z)$ is sectionally analytic in the complex plane. In addition, $\underline{R}(z,\mu)$ is an analytic function of z [see eq(21b)].

3. Fourier Transform Inversion and Singular Eigenfunction Expansion

It now becomes a relatively straightforward exercise to perform a Fourier inversion of eq(21a). For brevity, the full analysis is not presented here and the interested reader is referred to ref. 12 for further details. The final solution can be written as

$$\vec{\Psi}(x,\mu)=\pm\sum_{j=1}^{J}\underline{\Phi}(\pm\nu_j,\mu)\underline{M}^{-1}_{Lj\pm}e^{\mp x/\nu_j}\vec{q}+ \\ +\int_0^{\pm1}d\nu e^{\mp x/\nu}\left[\underline{\Phi}(\nu,\mu)\underline{M}_L^{-1}(\nu)\right]\vec{q} \qquad (24)$$

with $+$ for $x>0$ and $-$ for $x<0$ and

$$det\underline{\Lambda}_L(\nu_j)=0,\quad j\ =\ 1,2,...J$$

$$\underline{M}_{Lj\pm}^{-1} \equiv \frac{2}{\nu_j^2}\underline{g}_L^{-1}\left(\nu_j, \nu_j\underline{\Sigma}\right) adj\left[\tilde{\underline{\Lambda}}_L^*\left(\nu_j\right)\right]\left[\frac{d\left|\tilde{\underline{\Lambda}}_L^*\right|}{d\nu}\right]_{\pm\nu_j}^{-1}$$

$$\underline{M}_L^{-1}(\nu) \equiv \frac{1}{\nu}\left[\underline{\Lambda}_L^{+-1}(\nu)\underline{\Theta}(\nu\underline{\Sigma})\tilde{\underline{\Lambda}}_L^{*--1}(\nu)\right]$$

$$\underline{\Theta}(x\underline{D}) \equiv diag\left[\theta_1\left(d_1 x\right),...,\theta_G\left(d_G x\right)\right]$$

where

$$\theta_g\left(xd_g\right) \equiv \begin{cases} 1, & xd_g \in \left[-1/\sigma_g, 1/\sigma_g\right] \\ 0, & xd_g \notin \left[-1/\sigma_g, 1/\sigma_g\right]. \end{cases}$$

All other symbols are defined in ref. 12.

4. Numerical Implementation and Demonstration

While determining the solution directly in terms of singular eigenfunctions is theoretically satisfying, it is not so from a numerical viewpoint. To use the above analysis to gain some numerical leverage, a numerical demonstration will now be performed. The scalar flux as represented by the first moment

$$\vec{\Psi}(x) \equiv \frac{1}{2\pi}\int_{-\infty}^{\infty} dk\, e^{-ikx}\,\underline{\Psi}_0(z)\,\vec{q} \qquad (25)$$

where $\underline{\Psi}_0(z)$ is given by eq(14b) will be evaluated. The evaluation is performed via a numerical Fourier transform inversion as described in the author's various publications. The only new feature is an interation on the Gauss/Legendre quadrature order until each point is below a desired error.

The demonstration will be for a full scattering matrix with relatively high order anisotropy (up to $L = 20$). A fictitious set of cross sections is generated by

$$\begin{aligned} \Sigma_g &= \frac{2(g+1)}{G} \\ C_{g,g',l} &= c_S g_a^l \frac{2(g'+1)}{10G(g+g'+1)} \end{aligned} \qquad (26)$$

where a Henyey-Greenstein scattering phase function with asymmetry factor g_a has been assumed.

Table 1 shows a comparison of the inversion for 5 desired errors ε. This table is presented in order to provide confidence in the inversion algorithm as implemented in the

FORTRAN code **mg.f**. The problem considered was for 5 groups, g_a=0.95, c_s = 0.95 and L = 10 for point source emission (see below). Except for a single point out of a total of 100 points, the results are better than desired for all groups. This indicates the effectiveness of the quadrature order interation.

Typically, as the scattering becomes more forward peaked, the inversion has increasing difficulty in generating correct values. This is a result of the truncated Legendre series representation of the scattering kernel. To attempt to improve the solution, a Wynn-epsilon algorithm was applied to the sequence of solutions specified by the order L of the scattering approximation. Table 2 shows a comparison with and without acceleration for scattering orders up to 20 near and far from the source. The accelerated values (shaded columns) are remarkably improved over the original values especially near the source. However, they also begin degrade at high scattering order far from the source. Improvement by acceleration will be a subject of continued investigation.

Figure 1a,b shows the scalar flux for a plane source at x = 0 in groups 1 and 5 respectively. When the source is in group 5, the flux in that group is relatively larger than the other groups near the source position. Eventually, since group 5 has the highest interaction cross section, the flux will decay below values of the other groups at distances away from the source. Figure 2a,b shows the scalar flux for the same infinite medium for a decaying source for $x > 0$

$$S(x) = e^{-\alpha x}\Theta(x) \tag{27a}$$

whose transform is

$$S(k) = \frac{z}{\alpha z + 1} \ . \tag{27b}$$

The inversion now becomes

$$\vec{\Psi}(x) \equiv \frac{1}{2\pi}\int_{-\infty}^{\infty} dk\, e^{-ikx} S(k)\, \underline{\Psi}_0(z)\vec{q} \ . \tag{28}$$

The presence of the source in $x > 0$ is clearly evident as the flux does not decay as rapidly as without the source (see Fig.1). For this case, α was specified as 0.1. Finally, the scalar flux from a point source is displayed in Figs. 3a,b. This flux is given by the plane/point transformation

$$\begin{aligned} \vec{\Psi}_{pt}(r) &\equiv -\frac{1}{2\pi r}\frac{d}{dr}\left[\frac{1}{2\pi}\int_{-\infty}^{\infty} dk\, e^{-ikr}\, \underline{\Psi}_0(z)\vec{q}\right] \\ &\equiv \frac{1}{2\pi r}\left[\frac{1}{2\pi}\int_{-\infty}^{\infty} dk\, \frac{e^{-ikr}}{z}\, \underline{\Psi}_0(z)\,\vec{q}\right] \end{aligned} \tag{29}$$

Two cases of 25 groups and $L = 10$ were considered. The first was for a source in the fifth group and the second for a source in each group with source strength 1/g. The flux behavior is as expected. This demonstration indicates that benchmark quality results can be obtained for a nontrivial problem. Cylindrical and shell geometries can also be accommodated.

4. Conclusion

The solution to the multigroup neutron transport equations for isotropic source emission has been obtained as a singular eigenfunction expansion through a Fourier transform approach. This approach avoids the relatively obscure mathematics associated with singular eigenfunction and resolvant operators. For this reason, what has been presented has significant educational value. The resulting expression for the scalar flux was numerically evaluated using a numerical Fourier transform inversion. Selected results were presented to demonstrate that benchmark quality is achieved and that relatively comprehensive multigroup problems of 25 groups and moderately high order scattering ($L = 10$) could be treated. Computational times on an Ultra 5 Sun workstation for any of the benchmarks were modest with the last computation for the point source taking under 30 minutes.

References

[1] R. Zelazny and A. Kuszell, *Ann Phys*., **16**, 81(1961).
[2] A. Leonard and J.H. Ferziger, *Nucl. Sci.& Eng*., **26**, 170(1966).
[3] C.E. Siewert and P.S. Seith , *Jour. Nucl. Ener*., **21**, 383(1967).
[4] T.Yoshimura and Katsuragi, *Nucl. Sci.& Eng*., **55**, 297(1968).
[5] J.K. Shultis, *Nucl. Sci.& Eng*., **38**, 83(1969).
[6] R.J. Reith Jr and C.E. Siewert, *Nucl. Sci.& Eng*., **47**, 156(1972).
[7] K.M. Case and P.F. Zweifel, *Linear Transport Theory*, Addison-Wesley, Pub. Co., Reading MA, (1967).
[8] R.L. Bowden, S. Sancaktar and P.F. Zweifel, *Jour. Math. Phys*.,17, 76(1976).
[9] R.L. Bowden, S. Sancaktar and P.F. Zweifel, *Jour. Math. Phys*.,17, 82(1976).
[10] B.D. Ganapol, TTSP,29,43-69 (2000).
[11] B.D. Ganapol and K. Parsons, M&C Topical Meeting, Madrid Spain, (1999).
[12] B.D. Ganapol, *Nucl. Sci.& Eng*., **137**, 200(2001).

ε = 1.0e-02

x/gp	1	2	3	4	5
1.0000E-02	7.8827E+02	4.52**41**E-01	4.694**3**E-01	4.766**1**E-01	4.786**4**E-01
3.3400E+00	2.8247E-04	1.6674E-05	1.0812E-05	7.8654E-06	6.1751E-06
6.6700E+00	2.8283E-06	1.9566E-07	1.1261E-07	8.000**4**E-08	6.254**3**E-08
1.0000E+01	5.012**3**E-08	3.543**4**E-09	1.9974E-09	1.4187E-09	1.1093E-09

ε = 1.0e-03

1.0000E-02	7.8827E+02	4.524**1**E-01	4.6940E-01	4.7659E-01	4.786**4**E-01
3.3400E+00	2.8247E-04	1.6674E-05	1.0812E-05	7.8654E-06	6.1751E-06
6.6700E+00	2.8283E-06	1.9566E-07	1.1261E-07	8.000**2**E-08	6.253**8**E-08
1.0000E+01	5.0121E-08	3.5435E-09	1.9974E-09	1.4187E-09	1.1093E-09

ε = 1.0e-04

1.0000E-02	7.8827E+02	4.5238E-01	4.6940E-01	4.7659E-01	4.7862E-01
3.3400E+00	2.8247E-04	1.6674E-05	1.0812E-05	7.8654E-06	6.1751E-06
6.6700E+00	2.8283E-06	1.9566E-07	1.1261E-07	8.000**2**E-08	6.253**8**E-08
1.0000E+01	5.0121E-08	3.5435E-09	1.9974E-09	1.4187E-09	1.1093E-09

ε = 1.0e-05

1.0000E-02	7.8827E+02	4.5238E-01	4.6940E-01	4.7659E-01	4.7862E-01
3.3400E+00	2.8247E-04	1.6674E-05	1.0812E-05	7.8654E-06	6.1751E-06
6.6700E+00	2.8283E-06	1.9566E-07	1.1261E-07	8.0003E-08	6.2539E-08
1.0000E+01	5.0121E-08	3.5435E-09	1.9974E-09	1.4187E-09	1.1093E-09

ε = 1.0e-06

1.0000E-02	7.8827E+02	4.5238E-01	4.6940E-01	4.7659E-01	4.7862E-01
3.3400E+00	2.8247E-04	1.6674E-05	1.0812E-05	7.8654E-06	6.1751E-06
6.6700E+00	2.8283E-06	1.9566E-07	1.1261E-07	8.0003E-08	6.2539E-08
1.0000E+01	5.0121E-08	3.5435E-09	1.9974E-09	1.4187E-09	1.1093E-09

Table1. Inversion error comparison for 5 group approximation for a point source.

x = 1.0000000000000D-03

L/gp	1	1	11	11
1	1.3247E-02	1.3247E-02	7.0022E-03	7.0022E-03
2	1.9444E-02	1.7100E-02	9.5242E-03	8.6033E-03
3	1.5249E-02	1.6943E-02	7.8275E-03	8.5099E-03
4	1.8390E-02	1.7006E-02	9.0700E-03	8.5359E-03
5	1.5968E-02	1.7026E-02	8.1157E-03	8.5344E-03
6	1.7921E-02	1.7095E-02	8.8740E-03	8.5351E-03
7	1.6325E-02	1.7049E-02	8.2569E-03	8.5354E-03
8	1.7660E-02	1.7053E-02	8.7679E-03	8.5355E-03
9	1.6533E-02	1.7053E-02	8.3385E-03	8.5354E-03
10	1.7498E-02	1.7052E-02	8.7031E-03	8.5353E-03
11	1.6665E-02	1.7052E-02	8.3905E-03	8.5328E-03
12	1.7389E-02	1.7052E-02	8.6605E-03	8.5351E-03
13	1.6756E-02	1.7052E-02	8.4257E-03	8.5351E-03
14	1.7313E-02	1.7052E-02	8.6309E-03	8.5350E-03
15	-8.7499E-04	1.7052E-02	8.2609E-03	8.5351E-03
16	7.9649E-03	1.7052E-02	8.5123E-03	8.5351E-03
17	-2.3925E-03	1.7052E-02	8.2673E-03	8.5329E-03
18	-3.5814E-02	1.7052E-02	8.0407E-03	8.5353E-03
19	-1.0986E-01	1.7053E-02	7.1708E-03	8.5354E-03
20	-3.6065E-01	1.7053E-02	6.2033E-03	8.5354E-03

x = 10.0000000000000

1	6.3871E-07	6.3871E-07	2.7602E-08	2.7602E-08
2	8.5598E-07	1.1660E-06	3.0678E-08	3.2635E-08
3	9.2138E-07	9.4955E-07	3.1521E-08	3.1839E-08
4	9.2656E-07	9.1514E-07	3.1598E-08	3.1377E-08
5	9.2421E-07	9.2320E-07	3.1573E-08	3.1560E-08
6	9.2404E-07	9.2465E-07	3.1571E-08	3.1577E-08
7	9.2422E-07	9.2422E-07	3.1573E-08	3.1573E-08
8	9.2421E-07	9.2419E-07	3.1572E-08	3.1572E-08
9	9.2413E-07	9.2426E-07	3.1572E-08	3.1573E-08
10	9.4228E-07	9.2419E-07	3.1771E-08	3.1572E-08
11	9.2714E-07	9.2422E-07	3.1613E-08	3.1573E-08
12	4.9031E-06	9.2404E-07	7.4231E-08	3.1570E-08
13	-1.8616E-05	9.2428E-07	-1.7326E-07	3.1573E-08
14	3.9782E-03	9.2404E-07	4.2887E-05	3.1570E-08
15	-2.5383E-03	9.2422E-07	-2.8438E-05	3.1573E-08
16	1.8623E-02	9.2414E-07	2.6451E-04	3.1572E-08
17	-8.6321E-02	9.2420E-07	-1.0394E-03	3.1572E-08
18	9.0226E-01	9.2414E-07	1.0432E-02	3.1572E-08
19	-2.5762E+01	9.2422E-07	-2.8992E-01	3.1573E-08
20	3.7591E+02	9.2465E-07	4.2904E+00	3.1577E-08

Table 2. Comparison with and without Wynn-epsilon acceleration $G = 15$.

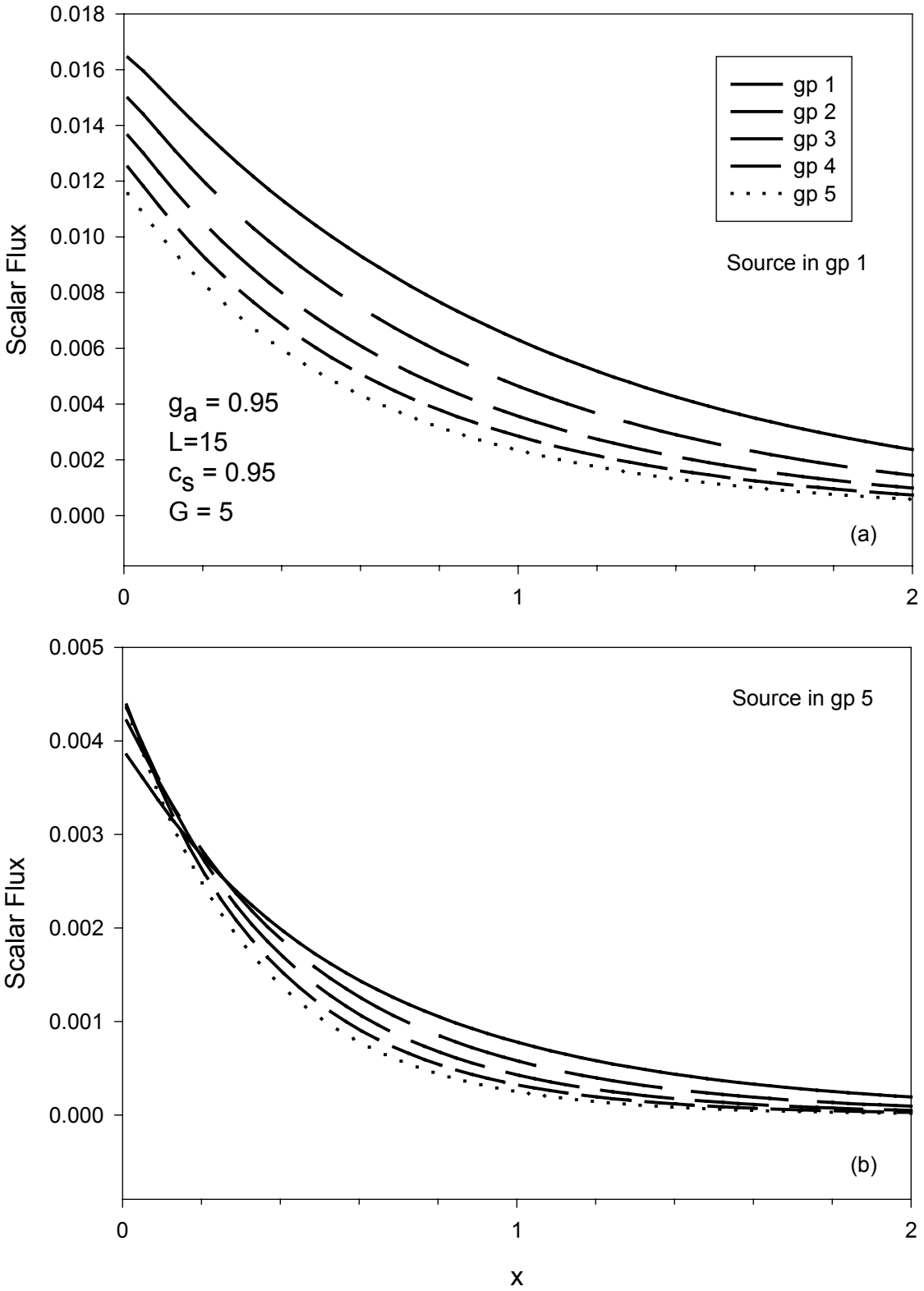

Fig. 1. Plane source at x = 0

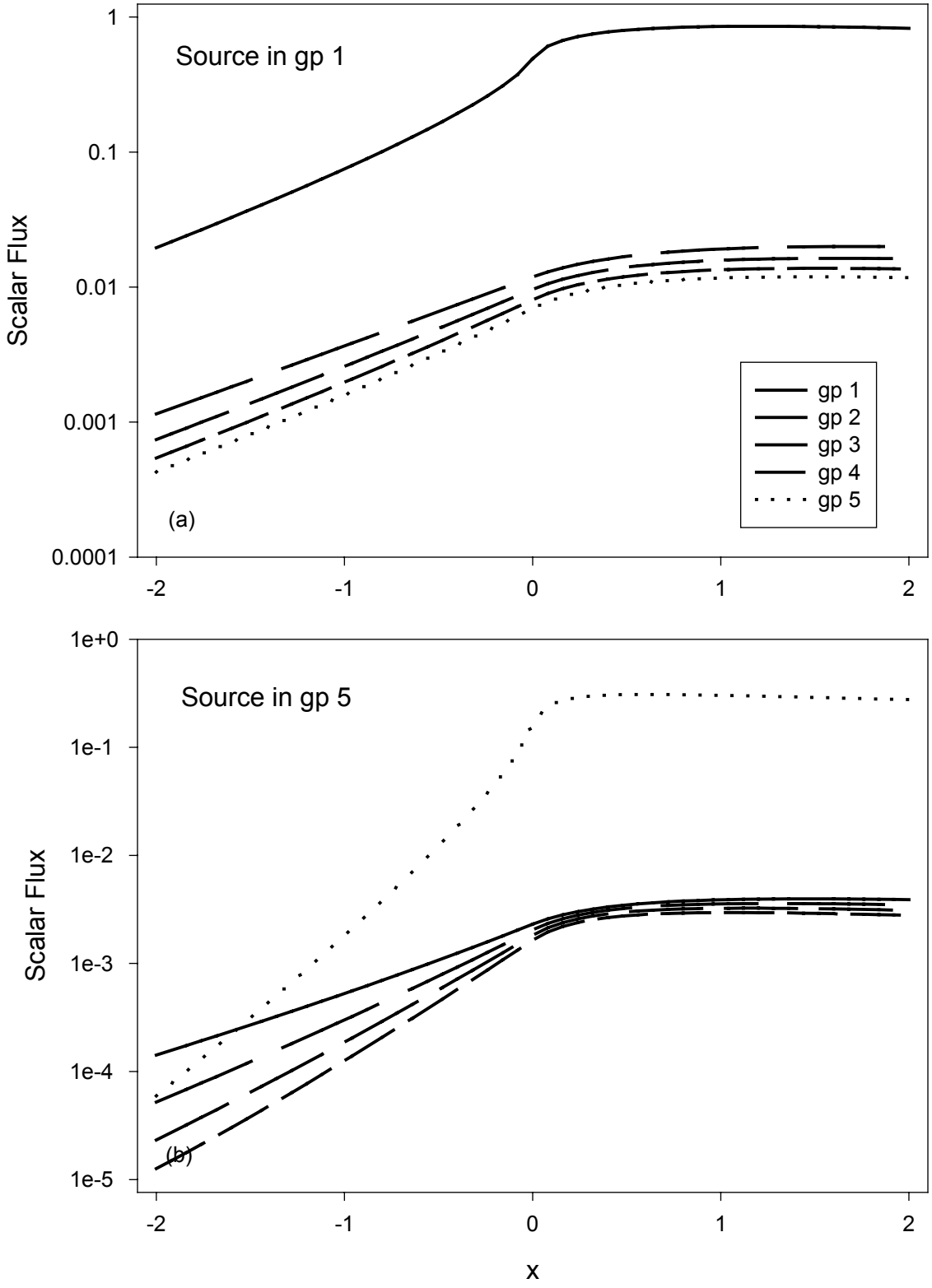

Fig. 2. Distributed source $e^{-\alpha x}\theta(x)$

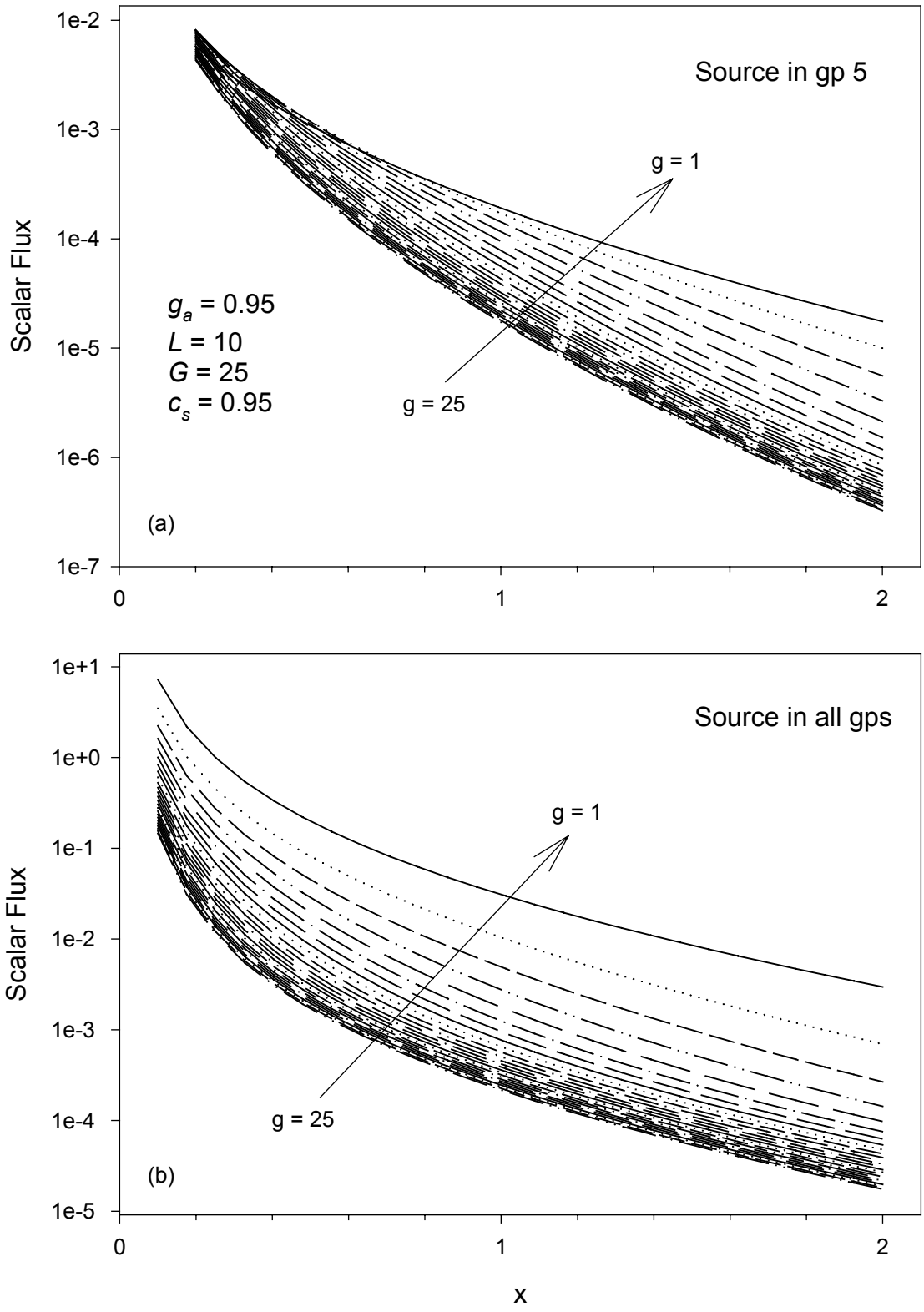

Fig. 3. Point source at r = 0